A Female *Homo erectus* Pelvis from Gona, Ethiopia

Scott W. Simpson,[1,2] Jay Quade,[3] Naomi E. Levin,[4,5] Robert Butler,[6] Guillaume Dupont-Nivet,[7] Melanie Everett,[8,9,10] Sileshi Semaw[9,10]*

Analyses of the KNM-WT 15000 *Homo erectus* juvenile male partial skeleton from Kenya concluded that this species had a tall thin body shape due to specialized locomotor and climatic adaptations. Moreover, it was concluded that *H. erectus* pelves were obstetrically restricted to birthing a small-brained altricial neonate. Here we describe a nearly complete early Pleistocene adult female *H. erectus* pelvis from the Busidima Formation of Gona, Afar, Ethiopia. This obstetrically capacious pelvis demonstrates that pelvic shape in *H. erectus* was evolving in response to increasing fetal brain size. This pelvis indicates that neither adaptations to tropical environments nor endurance running were primary selective factors in determining pelvis morphology in *H. erectus* during the early Pleistocene.

The modern human pelvis is uniquely modified to accommodate both bipedal locomotion and the birthing of large-brained offspring (*1*, *2*). The earliest known fossil hominid adult pelves are from small-bodied females (such as the 3.2-million-year-old *Australopithecus afarensis* specimen A.L. 288-1an/ao and the ~2.5- to 2.8-million-year-old *Au. africanus* specimen Sts14) that show anatomical adaptations to bipedal locomotion yet lack obstetric specializations. By the early Pleistocene, *Homo erectus* exhibited an absolute and relative increase in brain size, suggesting that the parturition of a large-brained fetus may have imposed novel selection on its pelvis. Few early *Homo* fossil pelvis fragments exist (*3*), and it is the 1.53-million-year-old juvenile male skeleton (KNM-WT 15000) from Kenya that has been central in assessing *H. erectus* pelvic morphology and body shape (*4*). The transversely narrow pelvis and torso reconstructed for this individual were suggested to be adaptations that enhanced locomotor effectiveness and thermoregulatory homeostasis in more open, semi-arid tropical environments (*4*, *5*). Estimates of female birth canal dimensions based on this fossil have been interpreted to suggest that *H. erectus* lacked derived obstetric modifications in the pelvis and that its small birth canal limited neonatal brain size (*3*, *6*) to a maximum of ~230 ml. This, in turn, was argued to have resulted in the birth of developmentally immature offspring that experienced rapid postnatal brain growth requiring a modern human–like degree of maternal investment and child-rearing behaviors (*6*).

Here we describe a nearly complete early Pleistocene adult female *H. erectus* pelvis and last lumbar vertebra (BSN49/P27a-d) from the upper Busidima Formation (*7*, *8*), dated 1.8 to <0.16 million years ago (Ma), in the Gona Paleoanthropological Research Project study area in the Afar Regional State, Ethiopia (Fig. 1). The BSN49 site is stratigraphically located between the Silbo Tuff (0.751 ± 0.022 Ma) and the base of the C1r polarity chron (1.778 Ma) (fig. S1). Consideration of the range of observed sediment accumulation rates in the Busidima Formation narrows the likely age of the fossil to 0.9 to 1.4 Ma (*8*). To date, *H. erectus* is the only hominid known from the early Pleistocene deposits in the Afar Depression. Early Acheulean artifacts are common at the BSN49 stratigraphic level. Analyses of carbon and oxygen stable isotopes from pedogenic carbonates and herbivore enamel from the BSN49 level indicate a semi-arid environment with a landscape dominated by C4 grasses and grazing herbivores (*8*).

The pelvis (Fig. 2) includes the sacrum and both os coxae with the first complete pubis from the early Pleistocene. Most of its distortion was produced by in situ fracture and carbonate cementation of the displaced fragments. The complete pelvis was reconstructed from high-resolution plaster casts. Despite minor residual asymmetry, the major functionally relevant dimensions and articular surfaces required little or no reconstruction and can be considered reliable for anatomical interpretation and mensuration (*8*).

The adult BSN49/P27 pelvis is transversely broad with laterally flaring ilia and anteriorly positioned acetabulocristal buttresses, long pubic rami, and a wide sciatic notch, which are all plesiomorphic characters shared with the australopithecines, other early (*3*) and middle (*9*, *10*) Pleistocene *Homo*, and Neandertals (*11*). The fossils attributable to *H. erectus* or early *Homo* [including KNM-WT 15000, KNM-ER 1808,

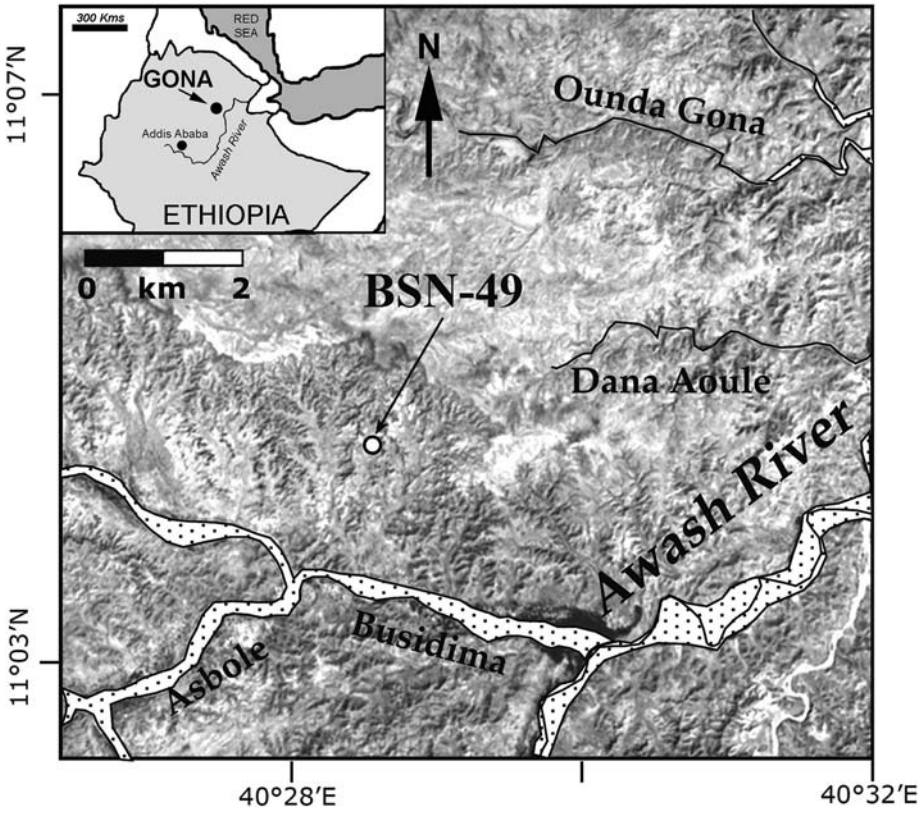

Fig. 1. Location of site BSN49. See (*8*) for additional information on site stratigraphy and tuff geochemistry.

[1]Department of Anatomy, Case Western Reserve University School of Medicine, Cleveland, OH 44106–4930, USA. [2]Laboratory of Physical Anthropology, Cleveland Museum of Natural History, Cleveland, OH 44106, USA. [3]Department of Geosciences/Desert Laboratory, University of Arizona, Tucson, AZ 85721, USA. [4]Department of Geology and Geophysics, University of Utah, Salt Lake City, UT 84112, USA. [5]Division of Geological and Planetary Sciences, California Institute of Technology, MC 100-23, Pasadena, CA 91125, USA. [6]Department of Physics, University of Portland, Portland, OR 97203–5798, USA. [7]Faculty of Geosciences, Utrecht University, Budapestlaan 17, 3584 CD Utrecht, Netherlands. [8]Department of Geological Sciences, Indiana University, Bloomington, IN 47407, USA. [9]The Stone Age Institute, 1392 West Dittemore Road, Gosport, IN 47433, USA. [10]Center for Research into the Anthropological Foundations of Technology (CRAFT), Indiana University, Bloomington, IN 47405, USA.

*To whom correspondence should be addressed. E-mail: ssemaw@indiana.edu

KNM-ER 3228, OH28, and UA-173/404+UA-466 (*3*, *12*)] span the early Pleistocene in Africa and exhibit laterally flaring ilia, wide (in terms of modern males) greater sciatic notches, tall thin pubic symphyseal faces, small auricular surfaces, and anteriorly placed iliac pillars. Except for overall size, the BSN49/P27 specimen is anatomically similar to these pelvis fossils (*8*). The BSN49/P27 pelvis shares with *Homo* such diagnostic characters (*8*) as an anteroposteriorly broadened birth canal, a thickened acetabulocristal buttress (iliac pillar), a sigmoid-shaped anterior inferior iliac spine, a shelf formed by attachment of the reflected head of the rectus femoris muscle, deepened fossa for the gluteus medius muscle, an increased height of the posterior ilium with an expanded retroauricular area, and angular elevation and anterior projection of the superior pubic rami (*13*). As in other *Homo* sacra, the BSN49/P27 alae are anteroposteriorly broad with marked periauricular excavation and a robust and projecting sacral tuberosity indicating a well-developed interosseous sacroiliac ligament complex: features that readily distinguish *Homo* from the australopithecines (*8*).

The BSN49/P27 acetabulae are small, with an estimated femoral head diameter of 33.4 to 36.8 mm (*8*)—substantially smaller than the femoral head of other early Pleistocene specimens [such as KNM-WT 15000: 44.9 mm (*14*)]. Regressions estimating femur length and stature based on the major load-bearing articular surfaces of the pelvis (*8*) predict a stature for the BSN49/P27 individual of 1.20 to 1.46 m, markedly shorter than the 1.85 m adult stature estimated for the male KNM-WT 15000 individual (*4*). Although *H. erectus* is widely characterized as apomorphically exhibiting an increase in stature and reduction in stature dimorphism, the data supporting this idea are surprisingly meager. With the recent discovery of *H. erectus* crania and postcrania from smaller individuals [such as KNM-OL 45500 (*15*), KNM-ER 42700 (*16*), and Dmanisi (*17*, *18*)], it is apparent that body size range in *H. erectus* has been underestimated, and a size "Rubicon" should not be part of the species diagnosis (*16*). The presence of very wide greater sciatic notches (*8*) and subpubic angle (table S5), everted ischia, rectangular pubic bodies with a ventral arc, a subpubic concavity, a large sacral angle (*19*), a nonprojecting sacral promontory, a symmetrically oval pelvic inlet, and a preauricular sulcus are all traits diagnostic of a female pelvis. Thus, the BSN49/P27 pelvis is from a short-statured *H. erectus* adult female.

The BSN49/P27 pelvis is obstetrically capacious for such a short-statured individual. The fossil's inlet circumference is within modern female ranges (*8*). The obstetrically important bispinous (pelvic midplane) and bituberal (pelvic outlet) transverse breadths of BSN49/P27 are greater than in most modern females (Fig. 3) (*8*). Size-normalized comparisons and multivariate analyses of the pelvic inlet and midplane demonstrate the obstetrically derived shape of the BSN49/P27 birth canal (Fig. 3, C and D) (*8*).

Humans are unusual among the hominoids in having a near identity in size between the neonatal head and the birth canal dimensions that places both mother and neonate at substantial risk of a traumatic birth. When these anatomical relationships in humans were used to estimate neonatal head size in *H. erectus*, it was seen that the BSN49/P27 pelvis was capable of birthing an offspring with estimated maximal brain volume of up to 315 ml (*8*)—over 30% greater than previously predicted from the KNM-WT 15000 pelvis (*6*), although this value is similar to growth-based estimates (*20*). Neonatal brain size was approximately 30 to 50% (the mean ratio is 34 to 36%) of early Pleistocene *H. erectus* adult brain size [~600 to 1067 ml (mean = 880 ml, n = 18 crania)] (*21*), an intermediate value between that of chimpanzees (~40%) and modern humans (~28%) (*20*). This new estimate of *H. erectus* neonatal brain size, in tandem with the revised age at death (~0.5 to 1.5 years) of the child's cranium from Perning (Mojokerto), Indonesia (<1.81 Ma) (*22*), suggests that *H. erectus* had a prenatal brain growth rate similar to that of humans but a postnatal brain and somatic growth rate intermediate between that of chimpanzees and humans (*23*).

The enlarged neonatal brain in *H. erectus* required a concomitant increase in the dimensions of their bony birth canal. Two nonexclusive means of enlarging birth canal size beyond the primitive *Australopithecus* condition (*1*) are an increase in female body size [larger females can have isometrically larger pelves (*24*)] or developmentally mediated changes in pelvic shape resulting in pelvic sexual dimorphism. Given this individual's short stature with a capacious birth canal and characteristically female pelvic shape,

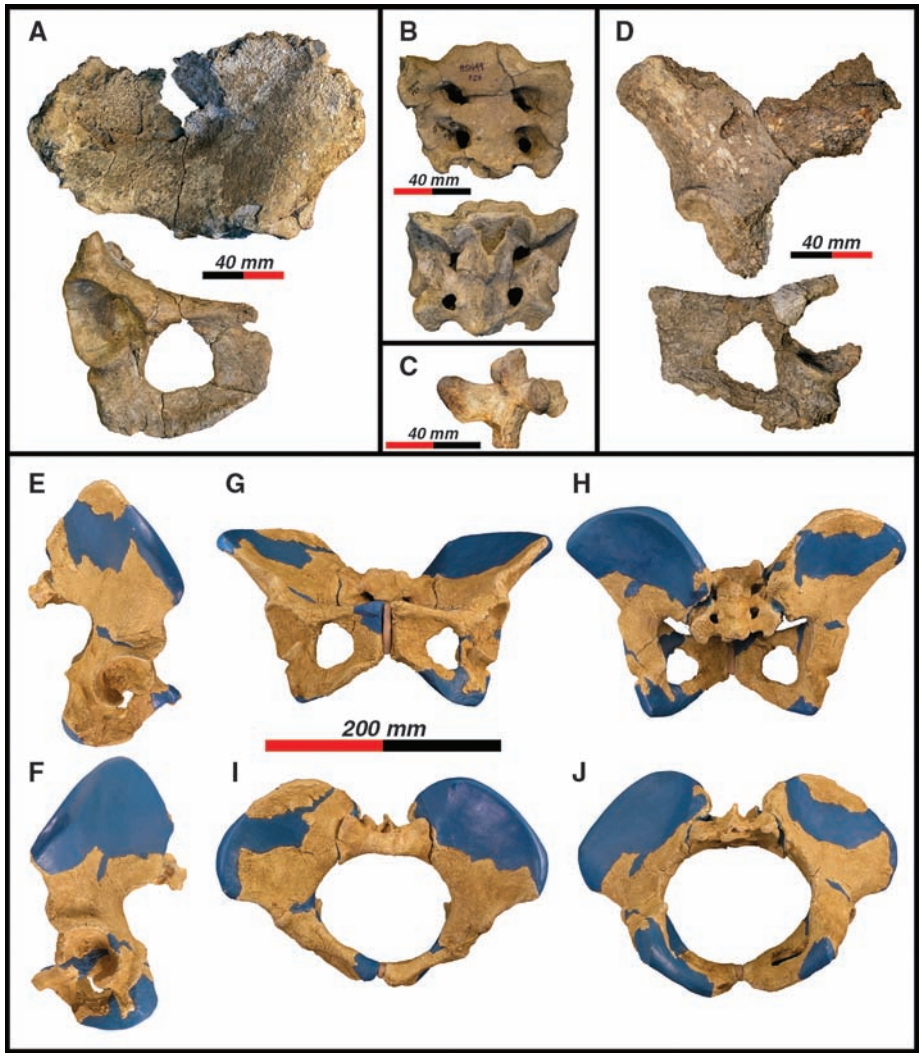

Fig. 2. Illustrations of major elements of the BSN49/P27 pelvis and lumbar vertebra and reconstruction of the pelvis. (**A**) Right os coxa with posterolateral view of the ilium and anterolateral view of an ischiopubic fragment. (**B**) Anterior and posterior views of the sacrum. (**C**) Right lateral view of the lumbar vertebra. (**D**) Posterolateral view of the left ilium and anterolateral view of the left ischiopubic fragment. (**E**) Right lateral view. (**F**) Left lateral view. (**G**) Anterior view. (**H**) Posterior view. (**I**) Pelvic inlet. (**J**) Pelvic outlet. The blue portions of the cast indicate areas that have been reconstructed or restored. Scale bar for (A) to (D), 40 mm; scale bar for (E) to (J), 200 mm.

it is clear that the latter applies. This resulted in a recognizably dimorphic pelvis by the early Pleistocene, with females demonstrating the distinctive obstetric anatomy required to deliver a large-brained offspring. This derived anatomy indicates that the fetal cephalic–maternal pelvic disproportion, which directly affects reproductive success, was a significant selective factor on female pelvic morphology at that time.

This individual's absolutely wide bi-iliac breadth (288 mm) is greater than the mean width of modern females and males from eight diverse populations (*8*, *19*, *25*, *26*), indicating that the BSN49/P27 individual had a very broad trunk. Its bi-iliac breadth is exceeded in the fossil record only by the very large middle and late Pleistocene pelves from Atapuerca, Spain (*9*), Jinniushan, China (*10*), and Kebara, Israel (*11*), which are specimens that retain the primitive condition of laterally flaring ilia. The only ancient pelvis that does not exhibit marked lateral flare is the reconstructed KNM-WT 15000 pelvis, a reconstruction that has been questioned (*3*, *9*).

Many anatomical changes in the human pelvis have occurred since the middle Pleistocene, including a narrowing of the interacetabular distance; an increase in the anteroposterior breadth of the birth canal, with shorter, elevated pubic rami; and a decrease in the degree of iliac flaring, leading to a reduction of the bi-iliac breadth (*13*). Some authors have suggested that these anatomical adaptations had their roots in the early Pleistocene as a locomotor adaptation by *H. erectus* to endurance running (*5*). The BSN49/P27 pelvis does not exhibit any of these anatomical modifications or others proposed to be adaptive responses to this behavior, such as tall stature, enlarged acetabulae, or a narrow torso. Clearly, improving locomotor effectiveness, as exhibited by a relative and absolute increase in lower limb length, was a component of the early *Homo* adaptive complex. However, the earliest fossil evidence of the modern human pelvis is documented about 100,000 years ago from Skhul, Israel, indicating both the recency of this morphology and the historical stability of the plesiomorphic transversely broad pelvis.

Modern humans display a relation between body shape and ambient temperature and humidity, with individuals living in more temperate and Arctic climates having absolutely and relatively broader torsos, and peoples in tropical arid/semi-arid areas possessing narrower trunks (*27*). The BSN49/P27 pelvis represents a short-statured, broad-hipped individual who would have had an extreme bi-iliac breadth/stature ratio characteristic of more temperate-adapted modern humans and not the tall narrow body form previously identified in *H. erectus* as an adaptation to tropical semi-arid environments (*4*, *8*). Thus, although early *Homo* lived in a diversity of environments, because of their unique pelvic shape they did not exhibit the same ecogeographic patterns of body form as seen in modern humans (*10*).

The first *H. erectus* fossils were found over 100 years ago. Additional *H. erectus* remains have since been recovered from numerous sites spanning over a million years, thousands of miles, and a wide diversity of ecological zones. These fossils have documented a substantial increase in endocranial capacity in *H. erectus* over their Pliocene ancestors. Despite this rich history, few complete fossil postcrania (*18*) have been recovered, and basic features of *H. erectus* body shape remain poorly understood. The transversely broad torso, clearly evident in this short individual, requires reappraisal of some current models of locomotor and ecogeographic adaptations in African early Pleistocene *H. erectus*. It is now clear that the *H. erectus* pelvis retained many elements of its australopithecine heritage, although substantially modified by the demands of birthing large-brained offspring.

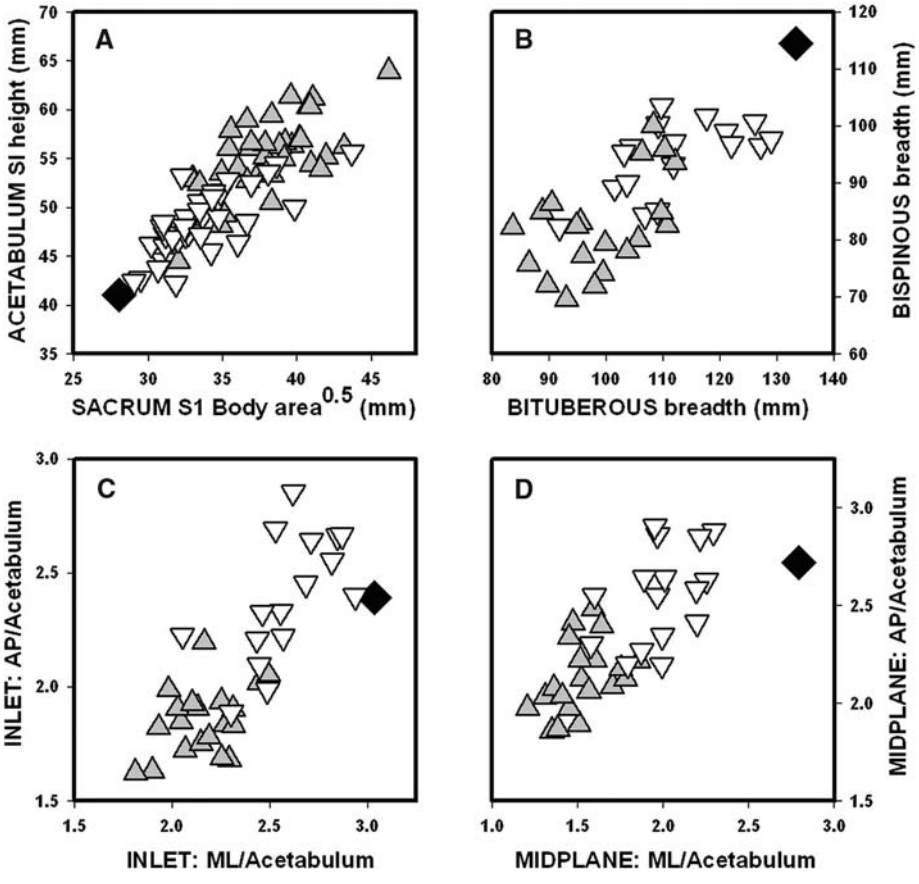

Fig. 3. Comparative pelvimetrics. (**A**) Plot of acetabulum superoinferior diameter with the square root of the sacral S1 body area (*8*). (**B**) Plot of bituberous breadth (pelvic outlet breadth) and bispinous breadth (pelvic midplane breadth). (**C**) Anteroposterior (AP) and mediolateral (ML) birth canal inlet dimensions normalized by acetabulum superoinferior diameter. (**D**) Anteroposterior and transverse birth canal midplane dimensions normalized by acetabulum superoinferior diameter. Human data are from The Hamann-Todd collection, Cleveland Museum of Natural History, Cleveland, Ohio. Open inverted triangles, females; gray triangles, males; black diamond, BSN49/P27.

References and Notes

1. C. O. Lovejoy, K. G. Heiple, A. H. Burstein, *Am. J. Phys. Anthropol.* **38**, 757 (1973).
2. R. G. Tague, C. O. Lovejoy, *J. Hum. Evol.* **35**, 75 (1998).
3. C. B. Ruff, *Am. J. Phys. Anthropol.* **98**, 527 (1995).
4. C. B. Ruff, A. Walker, in *The Nariokotome* Homo erectus *Skeleton*, A. Walker, R. Leakey, Eds. (Harvard Univ. Press, Cambridge, MA, 1993), pp. 234–265.
5. D. M. Bramble, D. E. Lieberman, *Nature* **432**, 345 (2004).
6. A. Walker, C. B. Ruff, in *The Nariokotome* Homo erectus *Skeleton*, A. Walker, R. Leakey, Eds. (Harvard Univ. Press, Cambridge, MA, 1993), pp. 221–233.
7. J. Quade *et al.*, *Geol. Soc. Am. Bull.* **116**, 1529 (2004).
8. Materials and methods are available as supporting material on *Science* Online.
9. J.-L. Arsuaga *et al.*, *Nature* **399**, 255 (1999).
10. K. Rosenberg, Z. Lü, C. B. Ruff, *Proc. Natl. Acad. Sci. U.S.A.* **103**, 3552 (2006).
11. Y. Rak, B. Arensburg, *Am. J. Phys. Anthropol.* **73**, 227 (1987).
12. L. Bondioli *et al.*, *J. Hum. Evol.* **50**, 479 (2006).
13. C. O. Lovejoy, *Gait Posture* **21**, 95 (2005).
14. C. Ruff, *Am. J. Phys. Anthropol.* **133**, 698 (2007).
15. R. Potts *et al.*, *Science* **305**, 75 (2004).
16. F. Spoor *et al.*, *Nature* **448**, 688 (2007).
17. G. P. Rightmire, D. Lordkipanidze, A. Vekua, *J. Hum. Evol.* **50**, 115 (2006).
18. D. Lordkipanidze *et al.*, *Nature* **449**, 305 (2007).
19. R. G. Tague, *Am. J. Phys. Anthropol.* **80**, 59 (1989).
20. J. DeSilva, J. Lesnik, *J. Hum. Evol.* **51**, 207 (2006).
21. R. L. Holloway, D. C. Broadfield, M. S. Yuan, *The Human Fossil Record: Brain Endocasts* (Wiley-Liss, Hoboken, NJ, 2004).
22. H. Coqueugniot, J.-J. Hublin, F. Veillon, F. Houët, T. Jacob, *Nature* **431**, 299 (2004).
23. C. Dean *et al.*, *Nature* **414**, 628 (2001).
24. R. G. Tague, *Am. J. Phys. Anthropol.* **127**, 392 (2005).

25. H. Correia, S. Balseiro, M. De Areia, *J. Comp. Hum. Biol.* **56**, 153 (2005).
26. D. Walrath, thesis, University of Pennsylvania, Philadelphia (1997).
27. C. B. Ruff, *Yearb. Phys. Anthropol.* **37**, 65 (1994).
28. The Gona Project thanks the Authority for Research and Conservation of Cultural Heritage of the Ministry of Culture and Tourism, and the National Museum of Ethiopia, for research permits and support. Support for this research was provided by the L. S. B. Leakey Foundation, National Geographic Society, Wenner-Gren Foundation, and NSF. We are grateful for the overall support of K. Shick and N. Toth (co-directors of CRAFT). We appreciate the hospitality of the Afar administration at Semera and our Afar colleagues from Eloha. We thank Y. Haile-Selassie and L. Jellema (Cleveland Museum of Natural History) for allowing us to examine materials in their care. Discussions with and comments by C. O. Lovejoy, R. G. Tague, Y. Haile-Selassie, G. Suwa, T. White, G. WoldeGabriel, B. Latimer, B. Asfaw, S. Standen, R. Byrne, and anonymous reviewers were helpful. A. Admasu's help at the National Museum of Ethiopia is appreciated.

Supporting Online Material
www.sciencemag.org/cgi/content/full/322/5904/1089/DC1
Materials and Methods
SOM Text
Figs. S1 to S11
Tables S1 to S10
References

22 July 2008; accepted 14 October 2008
10.1126/science.1163592

Slide into Action: Dynamic Shuttling of HIV Reverse Transcriptase on Nucleic Acid Substrates

Shixin Liu,[1] Elio A. Abbondanzieri,[1] Jason W. Rausch,[4] Stuart F. J. Le Grice,[4] Xiaowei Zhuang[1,2,3]*

The reverse transcriptase (RT) of human immunodeficiency virus (HIV) catalyzes a series of reactions to convert single-stranded viral RNA into double-stranded DNA for host cell integration. This process requires a variety of enzymatic activities, including DNA polymerization, RNA cleavage, strand transfer, and strand displacement synthesis. We used single-molecule fluorescence resonance energy transfer to probe the interactions between RT and nucleic acid substrates in real time. RT was observed to slide on nucleic acid duplexes, rapidly shuttling between opposite termini of the duplex. Upon reaching the DNA 3′ terminus, RT can spontaneously flip into a polymerization orientation. Sliding kinetics were regulated by cognate nucleotides and anti-HIV drugs, which stabilized and destabilized the polymerization mode, respectively. These long-range translocation activities facilitate multiple stages of the reverse transcription pathway, including normal DNA polymerization and strand displacement synthesis.

Retroviral reverse transcriptase (RT) is a multifunctional enzyme that catalyzes conversion of the single-stranded viral RNA genome into integration-competent double-stranded DNA. RT possesses several distinct activities, including DNA- and RNA-dependent DNA synthesis, DNA-directed RNA cleavage, strand transfer, and strand displacement synthesis, all of which are required to complete the reverse transcription cycle (fig. S1) (*1*, *2*). The enzyme first uses viral RNA as the template to synthesize minus-strand DNA (*3*, *4*), and the resulting DNA/RNA hybrid is then cleaved by the ribonuclease H (RNase H) activity of RT to produce short RNA fragments hybridized to nascent DNA (*5*, *6*). Specific RNA fragments, known as the polypurine tracts (PPTs), serve as primers for synthesis of plus-strand DNA from the minus-strand DNA template (*7*–*9*). Secondary structures present in the viral RNA genome, as well as the nontemplate strands hybridized to the DNA template, require RT to perform strand displacement synthesis during both minus- and plus-strand DNA synthesis (*10*–*16*).

As a major target for anti-HIV therapy, RT has been the subject of extensive research. Crystal structures, biochemical assays, and single-molecule analyses have suggested different modes of interaction between RT and nucleic acid substrates, providing snapshots of the nucleoprotein complexes that illuminate the functional mechanism of RT [e.g., (*17*–*25*)]. Nevertheless, how the enzyme-substrate complex acquires specific functional configurations and switches between different functional modes remains unclear. For example, how does RT efficiently locate the 3′ terminus of nascent DNA on a long duplex substrate to initiate DNA polymerization? This question is particularly important for a low-processivity polymerase such as RT, which must frequently locate the polymerization site after dissociation (*10*, *26*). Perhaps even more puzzling is how the dissociated RT locates the polymerization site during strand displacement synthesis, considering that the primer terminus may itself be displaced from the template by the competing nontemplate strand. Also, RT cleaves at many different sites within a DNA/RNA hybrid, but how it accesses these sites remains incompletely understood (*21*, *22*). A dynamic visualization of RT interacting with different substrates will help us address these questions and gain a more complete understanding of its function.

In this work, we used fluorescence resonance energy transfer (FRET) (*27*, *28*) to monitor in real time the action of individual HIV-1 RT molecules and their interactions with various nucleic acid substrates. We specifically labeled RT with the FRET donor dye Cy3 at either the RNase H domain (H-labeled) or the fingers domain (F-labeled) of its catalytically active p66 subunit (fig. S2A) (*2*, *29*, *30*). A $Glu^{478}\rightarrow Gln^{478}$ (E478Q) mutation was introduced to eliminate RNase H activity (*31*) and prevent degradation of the nucleic acid substrates during experiments. Nucleic acid substrates were labeled with the FRET acceptor dye Cy5 at various sites, specifically immobilized on a quartz surface, and immersed in a solution containing Cy3-labeled RT (fig. S2B) (*2*). Fluorescence from individual RT-substrate complexes was monitored with a total-internal-reflection fluorescence (TIRF) microscope by using an alternating laser excitation scheme (*32*). The observed FRET value allowed the binding configuration of the enzyme to be determined (fig. S2C) (*2*). Control experiments showed that neither dye labeling nor surface immobilization notably affected the enzyme activity (fig. S3) and that photophysical properties of the FRET dyes did not change appreciably when placed in proximity to the enzyme (fig. S4) (*2*).

To mimic substrates encountered by RT during minus-strand synthesis, we constructed a series of hybrid structures of various lengths, each consisting of a DNA primer and an RNA template with Cy5 attached to one of two sites: (i) near the 3′ end of the RNA template, which we define as the back end of the hybrid ("back-labeled," Fig. 1, A to C), or (ii) near the 5′ end of the RNA template and 3′ end of the DNA primer, which we define as the front end ("front-labeled," fig. S5, B and C) (*2*). On a 19–base pair (bp) hybrid, a length chosen to approximate its footprint on nucleic acid duplexes (*17*, *33*), RT bound in only one configuration: Binding of H-labeled RT to the back-labeled substrate yielded uniformly high FRET values (centered at 0.95) (Fig. 1A), indicating that RT bound with its RNase H domain close to the back end of the hybrid. Considering that the RNase H and polymerase active sites are at opposite ends of the substrate binding cleft of RT, this configuration places the polymerase active site of the RT over the 3′ terminus of the DNA primer, consistent with the polymerization-competent binding mode observed in crystal structures (*17*, *18*).

In contrast, two distinct binding modes were observed on longer DNA/RNA hybrids. H-labeled RT bound to back-labeled 38-bp hybrid yielded two FRET peaks centered at 0.95 and 0.39, re-

[1]Department of Chemistry and Chemical Biology, Harvard University, Cambridge, MA 02138, USA. [2]Department of Physics, Harvard University, Cambridge, MA 02138, USA. [3]Howard Hughes Medical Institute, Harvard University, Cambridge, MA 02138, USA. [4]HIV Drug Resistance Program, National Cancer Institute, Frederick, MD 21702, USA.

*To whom correspondence should be addressed. E-mail: zhuang@chemistry.harvard.edu